ELSEVIER

Polymer 42 (2001) 4837–4844

polymer

www.elsevier.nl/locate/polymer

Effect of structure on second harmonic generation in molecularly doped poly(ethylene oxide)/*atactic*-poly(methylmethacrylate) blends

A.D. Grishina[a], L.Y.A. Pereshivko[a], T.V. Krivenko[a], V.V. Savel'ev[a], J. Vernel[b], R.W. Rychwalski[b], A.V. Vannikov[a,*]

[a]*A.N. Frumkin Institute of Electrochemistry, Russian Academy of Science, Leninsky Prospekt 31, 117071 Moscow, Russia*
[b]*Department of Polymeric Materials, Chalmers University of Technology, SE-412 96 Göteborg, Sweden*

Received 3 July 2000; accepted 30 November 2000

Abstract

The second harmonic generation in *atactic*-PMMA containing *para*-nitrosodimethylaniline (NDMA) and in PEO/PMMA blends containing 2, 6, 16 and 25 vol.% PEO doped with 4-anilino-4′-nitroazobenzene (Disperse Orange-3 dye, DO-3), is investigated. This work confirms an earlier finding that information on the mechanism governing the kinetic characteristics of the second harmonic signal decay in corona poled polymer systems can be obtained only through the simultaneous measurements of both the second harmonic signal and the surface potential, published by us. The results of the study concern the dependence of the second harmonic relaxation time on the temperature, the concentration of the optically non-linear molecules in the polymer matrix and the composition of the blends. The surface potential and second harmonic signal relaxation time, τ_e, decrease more than 5×10^4 times when the amount of PEO in the blend is increased from 2 to 25%, while the rotational diffusion time always remains less than τ_e. Addition of hole transporting molecules into the optically non-linear composition based on 2 vol.% PEO speeds up the surface potential decay and strengthens the DO-3 rotational relaxation process. It is established that in the blends with low PEO concentration molecular alignment increases significantly around the temperature at which the cubic coefficient of thermal expansion starts to increase.

Keywords: Non-linear optics; Second harmonic generation; Surface potential

1. Introduction

Optical non-linearity and second harmonic generation (SHG) can be achieved in amorphous polymer systems (the host) by adding certain molecular dipoles (the guest chromophores) and then poling the samples in a high electric field to obtain a preferential orientation of the guest dipoles. High fields can be obtained by using contact electrode or corona poling. The latter is the most commonly used technique for polymer systems [1,2]. After the corona or contact electrode poling residual charges retard randomisation of chromophores and thus hinder the second harmonic (SH) signal decay in the polymer film [3]. In a number of studies it is shown that the presence of a trapped charge can affect the performance of non-linear optical (NLO) polymers in several ways. The presence of the trapped charge has been suggested to be a possible reason for, first, the great difference in orientation relaxation times in a polymer as measured by SH techniques and by dielectric relaxation [4,5], secondly, the influence of the poling field magnitude on the relaxation time of polymers [6] and thirdly, the "memory effect" in which the SH signal relaxation time of a poled polymer film increases with the number of poling cycles performed [7–9]. These studies were carried out without measuring the electrical parameters of optically non-linear polymers.

Charge effects in *para*-nitroaniline doped PMMA thin films were studied by Pauley et al. [10] using the simultaneous measurements of the current through a poling circuit and the SH signal. The contact electrode poling was used. It was shown that even after grounding the electrodes after poling the SH signal decay can be associated with the orientational relaxation of the oriented dipoles. This is strongly affected by the charge injected by the electrodes and trapped in the interior of the film [10].

The trapped charge influences the SH signal more strongly in the case of corona poling. The corona poling was used to study the SHG in 4-(dimethyl-amino)-4′-nitrostilbene (DANS) doped PMMA [11]. For the first time electric field effects were examined by simultaneously measuring the SH signal (during and following poling)

* Corresponding author. Fax: +7-95-952-08-46.
E-mail address: van@elchem.ac.ru (A.V. Vannikov).

0032-3861/01/$ - see front matter
PII: S0032-3861(00)00882-X

and the surface voltage decay (following poling). The residual electric field was found to increase the temporal stability of the SH signal [11]. Similar results were obtained in studies dealing with Dispersion Orange (DO-3) doped poly(vinyl acetate) [12], PMMA [13] and poly(ethylene oxide) (PEO)/*atactic*-PMMA blends [14] at room temperature by measuring both the SH signal and the surface voltage decay. It was also shown that the kinetics of SH relaxation is entirely determined by the surface potential decay. Therefore only parallel time-dependent measurements of the SH signal and the surface potential of poled NLO films allow evaluation of the real contribution of dopant molecule rotational diffusion to the SH signal decay.

This work concerns the main factors governing the kinetic characteristics of the decay in SHG efficiency in two different polymer systems. The first system consists of PMMA doped with *para*-nitrosodimethylaniline (NDMA: $(CH_3)_2N–C_6H_4–NO$) NLO chromophore. The second one is a PEO/PMMA blend with a rather low PEO content doped with DO-3 ($H_2N–C_6H_4–N{=}N–C_6H_4–NO_2$) dye. The dependence of the physical characteristics of the PEO/PMMA blends, namely the glass transition temperature, T_g, the temperature $T_{g,vol}$ at which the coefficient of cubic thermal expansion undergoes changes, the free volume and some other parameters of the systems were investigated as a function of PEO content [15–17]. A relationship between the SH signal relaxation kinetics and the surface potential for PEO/PMMA blends doped with DO-3 dye at room temperature was described earlier [14]. In the present work a relationship between the SH relaxation characteristics and the surface potential was analysed after heating the samples to different temperatures up to T_g. Changes in the relaxation processes are discussed in terms of the free volume.

2. Experimental

PEO/PMMA blends containing 2, 6, 16 and 25 vol.% PEO were prepared. The materials, sample preparation, purification procedures and experimental set-up used in this work are described elsewhere [12,14–16]. NDMA was purified by re-crystallisation from ethanol. Acetone (reagent grade) was purified by distillation. Polymer layers 3–4 μm thick were formed on indium–tin-oxide (ITO) coated glass plates by spin casting from acetone solutions. The layers were dried by heating for 3 h at 60°C and by storage in vacuum at about 10^{-5} Pa for 24 h.

The specimens were irradiated by pulses of Nd:YAG laser light at 1064 nm wavelength with a beam diameter of 0.3 cm, an energy of about 50 mJ pulse^{-1} and a pulse duration of 10 ns. A negative surface potential, U, producing a DC poling electric field, E, across the specimen was applied using the corona discharge [1]. A steel wire held 1 cm away from the polymer surface was negatively biased at $V_c = 4$ kV. The ITO substrate was used as a grounded electrode. Ions deposited on the polymer surface produced a surface charge. The SH intensity (at a wavelength of 532 nm) generated by the polymer layer was measured using a photoamplifier and a digital voltmeter. The digital voltmeter indications (mV) are proportional to SH intensities, I, where $I^{0.5} \propto \chi^{(2)}$ and $\chi^{(2)}$ is the second-order macroscopic polarisability. The voltage was recorded after each laser pulse. The surface potential decay was measured on the same specimen in parallel experiments. During the measurements the temperature was changed by an air flow directed onto the glass substrate. The relative absorption spectra in the visible region were recorded with a DU-7 (Beckman) spectrophotometer.

3. Results and discussion

3.1. PMMA doped with NDMA

The absorption spectrum for NDMA in PMMA matrix has a maximum at 420 nm and short and long wavelength thresholds at 330 and 510 nm, respectively. The composition is transparent in the region of the second harmonic at 532 nm. The following two reasons gave us grounds to expect SHG for NDMA molecules. First $\chi^{(2)}$ is proportional to $[W^2 - (2\hbar\omega)^2]^{-1}$ where W is the energy difference between the ground state and the first excited state for the NDMA molecule and $2\hbar\omega$ is the SH photon energy [18,19]. Since $W \approx 2.66$ eV and $2\hbar\omega = 2.33$ eV the difference $W^2 - (2\omega)^2$ is small and $\chi^{(2)}$ is significant. Second, the NDMA molecule has a sufficiently large dipole moment in the ground state ($\mu_0 \sim 6.8$ debye) to promote alignment of the optically non-linear molecules in the DC electric field.

The SH signal arises only upon application of the DC field E which is defined by the surface potential U ($E = U/d$, where d is the specimen thickness). Fig. 1 shows a plot of the square root of the SH intensity and the surface potential (in normalised units) versus the time after switching off the corona discharge. The $(I/I_0)^{0.5}$ and U/U_0 decay curves coincide and they can be fit by the same equation:

$$(I/I_0)^{0.5} \text{ (and } U/U_0) = \alpha \exp(-t/\tau_{e1}) + (1 - \alpha) \exp(-t/\tau_{e2}). \quad (1)$$

Here I_0 and U_0 are the SH intensity and the surface potential immediately after switching off the corona discharge and τ_{e1} and τ_{e2} are the relaxation times for the fast and slow terms. The coefficient α and the relaxation times τ_{e1} and τ_{e2} in Eq. (1) for different concentrations of NDMA are given in Table 1. The increase of the coefficient α and the shortening of the relaxation times τ_{e1} and τ_{e2} with increasing NDMA concentration can be observed in Table 1 and in Fig. 1. The relaxation time τ_e is related to the conductivity, σ, by the following equation [20]:

$$\sigma \text{ (S cm}^{-1}) = 8.85 \times 10^{-14} \epsilon/\tau_e \text{ (s)}. \quad (2)$$

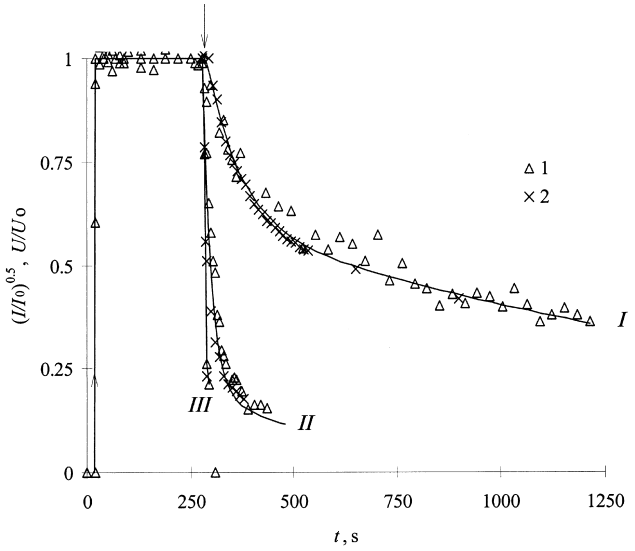

Fig. 1. (1) The normalised second harmonic intensity $(I/I_0)^{0.5}$ and (2) surface potential U/U_0 kinetic curves after switching the corona discharge on and off. PMMA films contain NDMA at molar concentrations of: (I) 0.42, (II) 1.75 and (III) 3.0. The solid lines follow Eq. (1) with α, τ_{e1} and τ_{e2} as given in Table 1.

Here ϵ is the dielectric constant of the polymer film. The conductivity increases with increasing NDMA concentration. This leads to a decrease in the DC surface potential, U_0, and hence the applied electric field $E_0 = U_0/d$. In fact, if one neglects both the surface conductivity and charge emission from the specimen surface to the surrounding gas phase then the DC surface charge density Σ obeys the expression $d\Sigma/dt = I - J = 0$ where I [$= k(V_c - U_0)(V_c - V_0 - U_0)$] is the corona DC current density on the specimen [21], J ($= U_0\sigma/d$) the current density through the bulk specimen, V_c($\approx$ 4000 V) the potential applied to the wire (see above), V_0 the threshold potential for the onset of the corona discharge and k a constant. The value of U_0 is not higher than 200 V and therefore $(V_c - U_0) \approx V_c$. Hence it follows that $kV_c(V_c - V_0 - U_0) - U_0\sigma/d = 0$ and therefore:

$$U_0 = V_c(V_c - V_0)[V_c + (\sigma/kd)]^{-1}. \quad (3)$$

The stationary potential is equal to $U_0 \approx (V_c - V_0)$ when σ is low ($V_c \gg \sigma/kd$) but it decreases with increasing σ when $V_c \leq \sigma/kd$.

The average distance r between the NDMA molecules at the concentrations used is 8–15 Å. When r is less than 15 Å hole conductivity with the NDMA molecules as transport centres can be expected. The bi-exponential decay of the surface potential shows the presence of two processes. According to one theory [22] the charge carriers are self-trapped or localised simply on transport centres by the polarising influence of the field of their own charge during the initial fast stage of the decay process. The following slow decay may arise from a thermal hopping process under the classical laws of diffusion. Simultaneously the NDMA molecules serve as NLO chromophores responsible for the SHG. As mentioned earlier, the close matching of the $(I/I_0)^{0.5}$ and U/U_0 decay curves after switching off the corona discharge is an indication that the SH decay characteristics are entirely defined by the surface potential.

Table 1
Dependence of α, τ_{e1} and τ_{e2} in Eq. (1) on NDMA concentration

NDMA (M)	α	τ_{e1} (s)	τ_{e2} (s)
0.42	0.4	80	1800
1.75	0.8	20	360
3.0	1.0	6	

Generally the SH relaxation kinetics results from both the rotational diffusion of molecules (relaxation time τ_{rot}) and the surface potential decay (relaxation time τ_e). The first mechanism is observed in the case when the rotational diffusion of the optically non-linear molecules is restricted and $\tau_{rot} > \tau_e$ in a polymer bulk. Then the relaxation process after switching off the corona discharge is described by the following bi-exponential dependence [2,23]:

$$I^{0.5} = A\exp(-t/\tau_{rot1}) + B\exp(-t/\tau_{rot2}) + C\,E_0\gamma. \quad (4)$$

Here A, B and C are constants proportional to the concentration of the optically non-linear molecules, $CE_0\gamma$ is a contribution due to the DC electric-field-induced third-order effect and γ the molecular third-order polarisability. The second mechanism is observed when $\tau_e > \tau_{rot}$ and the surface potential controls the second harmonic kinetic characteristics. Then DC electric-field-induced second harmonic (EFISH) takes place [24] and:

$$I^{0.5} \propto cE[(\beta\mu_0/5kT) + \gamma]. \quad (5)$$

Here c is the concentration of the optically non-linear molecules, and β the molecular second-order polarisability. In this case the decrease of the surface potential, U, and hence the DC electric field decay after switching off the corona discharge causes the SH signal decay according to Eq. (1).

The value of $I^{0.5}$ increases by a factor of 2.2 on increasing the concentration of NDMA from 0.42 to 1.75 M and remains nearly constant when the NDMA concentration is further increased to 3.0 M. The absence of a linear dependence of $I^{0.5}$ on the NDMA concentration c in these experiments is caused by the growth of σ with the increase in the NDMA concentration. In turn, this is accompanied by a decrease in the DC surface potential and hence by a decrease in the DC electric field E_0 according to Eq. (3).

3.2. PEO/PMMA blends containing DO-3 dye

Fig. 2a and b shows the decay of the normalised SH signal $(I/I_0)^{0.5}$ and the surface potential U/U_0 for the 2% PEO/PMMA blend doped with DO-3 in concentration up to 0.5 M after switching off the corona discharge. Samples became opaque at a DO-3 concentration $\geq$0.5 M due to the formation of a crystalline phase. The temporal decay of both $(I/I_0)^{0.5}$ and U/U_0 does not depend on the DO-3

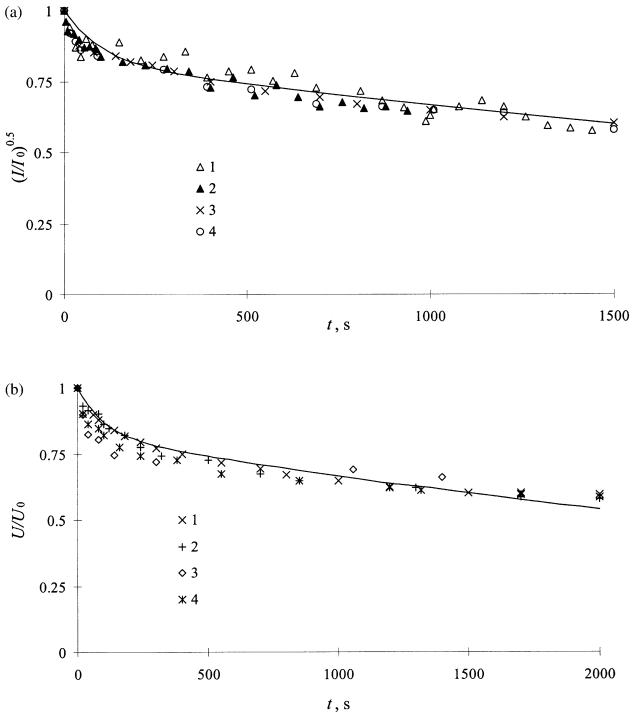

Fig. 2. (a) The $(I/I_0)^{0.5}$ and (b) U/U_0 decays after switching off the corona discharge. The 2 vol.% PEO/PMMA blend contains DO-3 at molar concentrations of: (1) 0.1, (2) 0.2, (3) 0.3 and (4) 0.4. The solid lines follow Eq. (1) with α, τ_{e1} and τ_{e2} as given in Table 2.

concentration. Thus, the DO-3 dye concentration is so small that electron–hole transport is not realised. The temporal decay of these characteristics is determined by ionic conductivity in the blend. The common bi-exponential dependence (Eq. (1)) with parameters $\alpha = 0.18$, $\tau_{e1} = 100$ s and $\tau_{e2} = 4800$ s (the solid curves in Fig. 2a and b) fits both the $(I/I_0)^{0.5}$ and U/U_0 experimental decay curves well.

In the following section, the basic second characteristics are given for the 2, 6, 16 and 25 vol.% PEO/PMMA polymer layers containing 0.4 M DO-3. The program for the SHG measurements consisted of three stages. In stage 1 the SH intensity and the surface potential were measured on switching the corona on and off. The measurements for the 2% blend shown in Fig. 2 are referred to below as "measured before heating". The measurement results corresponding to stages 2 and 3 are in Fig. 3. In stage 2,

Table 2
Values of α, τ_{e1} and τ_{e2} in Eq. (1) measured before and after heating to T (°C) for blends containing different amounts of PEO and 0.4 M DO-3

PEO	Before heating			T (°C)	After heating		
Vol.%	α	τ_{e1} (s)	τ_{e2} (s)		α	τ_{e1} (s)	τ_{e2} (s)
2	0.18	100	4800	75	0		> 720 h
6	0.5	90	4200	75	0.15	90	> 410 h
16	0.5	45	1200	70	0.5	45	1200 s
25	0.7	20	500	70	0.7	20	500 s

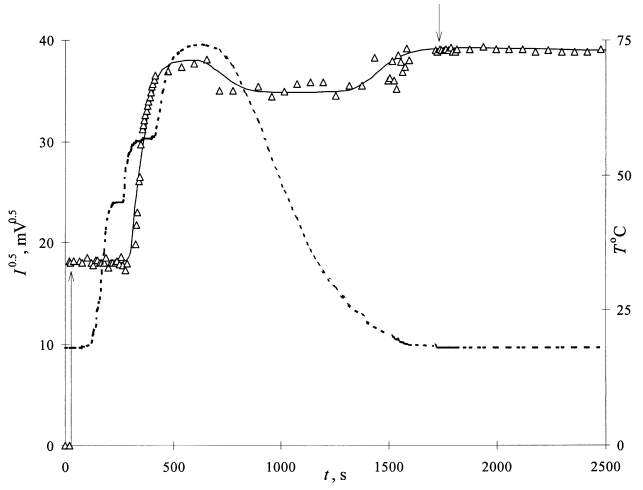

Fig. 3. The temporal dependence of $I^{0.5}$ (solid line) after switching the corona discharge on and off (arrows up and down, respectively). The dotted line shows the specimen temperature. The 2 vol.% PEO/PMMA blend contains 0.4 M of DO-3.

the SH signal intensity was measured during the corona discharge during heating to temperatures between 50 and 75°C followed by cooling to room temperature. In stage 3 the $(I/I_0)^{0.5}$ and U/U_0 decay curves were registered at room temperature after switching off the corona discharge. These measurements are referred to below as "measured after heating". In Table 2 the parameters α, τ_{e1} and τ_{e2} in Eq. (1) measured before and after heating for different content of PEO are given. The maximal temperatures are also shown in Table 2.

Fig. 3 includes the temperature run and the SH signal intensity for the 2% blend. The SH signal appears immediately after switching on the corona discharge and does not change during heating the sample from room temperature to 45°C. It sharply increases within the temperature region 52–57°C which is far below the glass transition temperature, T_g(≈ 90°C, measured calorimetrically, mid-point T_g). The sharp increase in the SH signal correlates well with the temperature at which the cubic coefficient of thermal expansion starts increasing strongly and departs from the glassy asymptote. This was determined by means of mercury-in-glass dilatometry. PMMA and the 6% blend were slowly cooled at a rate of −0.1 K/min and the external volume was recorded. Typically for glasses in their T_g-region a characteristic bi-tangential volume–temperature diagram is recorded and the point of departure was determined. The point was found to be at 57°C and 42°C for the PMMA and the 6% PEO blend, respectively [17]. For the 2% blend this point is at about 52°C. Thus we conclude that it is the increase in the free volume in the 2% PEO/PMMA blend that induces the alignment of a considerable portion of the DO-3 molecules in the DC electric field. This temperature is near to the secondary β transition temperature ($T_β$) for PMMA [23,25]. This effect can be expected if the average free volume of a microcavity is near to the van der Waals

volume of the optically non-linear constituent. The DO-3 molecule van der Waals volume given by Brower and Hayden [26] is equal to 202 Å^3 (the radius of an equivalent sphere is 3.64 Å). The average radius of the microcavity free volume in the PEO/PMMA blends is 2.7 Å for the 16% PEO sample and 2.83 Å for the 25% PEO content [15,16]. Since the DO-3 radius is larger than the average microcavity radius, filling these microcavities with the chromophore is sterically hindered. The microcavities have been shown to have a broad distribution of free volume sizes [15]. For example, the microcavity volume changes from 27 Å^3 to maximal values, V_{max}, reaching 204–214 and 244–305 Å^3 for 18 and 50 vol.% PEO, respectively [15]. Hence, the examined compositions contain microcavities of which only some exceed the DO-3 van der Waals volume. For this reason one can expect the restriction of the rotational diffusion of optically non-linear molecules at room temperature.

As can be seen in Fig. 3, following heating at 75°C the value of $I^{0.5}$ measured at room temperature does not decrease after switching off the corona discharge. Neither does U decrease. For the same specimen $I^{0.5}$ and U decrease by half after storage in vacuum for 30 days at room temperature.

Like the 2% blend behaviour described earlier, the $I^{0.5}$ decay measured at 20°C for the 6% PEO/PMMA blend doped with DO-3 after switching off the corona discharge changed greatly as a result of heating. Fig. 4 shows the $(I/I_0)^{0.5}$ and U/U_0 decay after switching off the corona discharge before the heating. The U/U_0 decay was measured for DO-3 doped and dopant-free samples. Eq. (1) with $\alpha = 0.5$, $\tau_{e1} = 90$ s and $\tau_{e2} = 4200$ s describes the experimentally measured behaviour well. The complete coincidence of the U/U_0 temporal dependencies for the DO-3 doped and dopant-free blends in Fig. 4 demonstrates that the polymer composition rather than the DO-3 dopant is responsible for the bulk conductivity. The contribution of the slow component $(1 - \alpha)$ in Eq. (1) increases from 0.5 before the heating to 0.85 after heating with the corona discharge at 75°C for 5 min (Table 2). The values of $I^{0.5}$ and U decreased by half after storage of the sample in vacuum for 17 days at room temperature.

The heating slightly alters the contributions to the fast and slow mechanisms of the $(I/I_0)^{0.5}$ relaxation for blends containing more than 16% PEO. The SH signals measured at room temperature for the 16% PEO blend before and after heating at 70°C are shown in Fig. 5 as well as the U/U_0 decay for the DO-3 doped and dopant-free blends. The $(I/I_0)^{0.5}$ decay curve measured before heating lies somewhat above the curve measured after heating. Both the curves are close to the surface potential decay curve for the dopant-free blend. The solid curve in Fig. 5 follows Eq. (1) with $\alpha = 0.5$, $\tau_{e1} = 45$ s and $\tau_{e2} = 1200$ s. The U/U_0 decays for the dopant-free PEO/PMMA blends correspond to an ionic mechanism of conductivity. The U/U_0 relaxation time shortens as the PEO content is increased (see Table 2). This indicates that PEO generates ionic conductivity in the blends. The explanation of the ionic nature of the conductivity requires a separate investigation.

The $I^{0.5}$ decay of the 25% blends doped with 0.4 M DO-3 is shown in Fig. 6. The SH signal drops to zero at 70°C. The $(I/I_0)^{0.5}$ decay curves measured at room temperature before and after heating (see Fig. 6, parts 1 and 2) are identical and

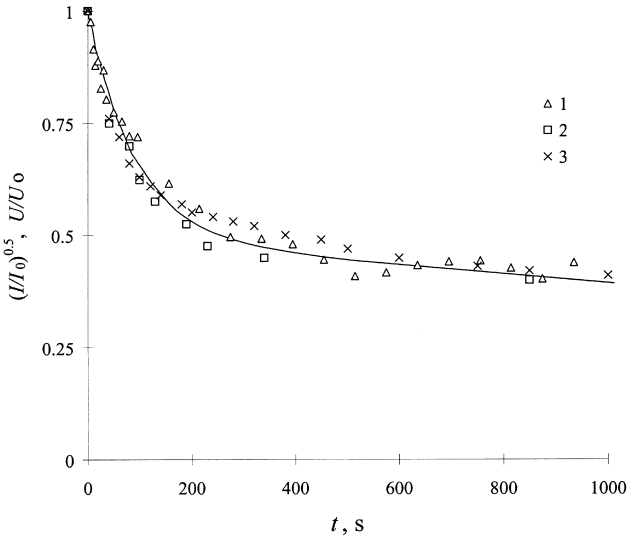

Fig. 4. (1) The $(I/I_0)^{0.5}$, (2) and (3) U/U_0 decays at room temperature after switching off the corona discharge. (1) and (2) 6 vol.% PEO/PMMA blend contains 0.4 M of DO-3 and (3) dopant-free. The solid line follows Eq. (1) and α, τ_{e1} and τ_{e2} are given in Table 2.

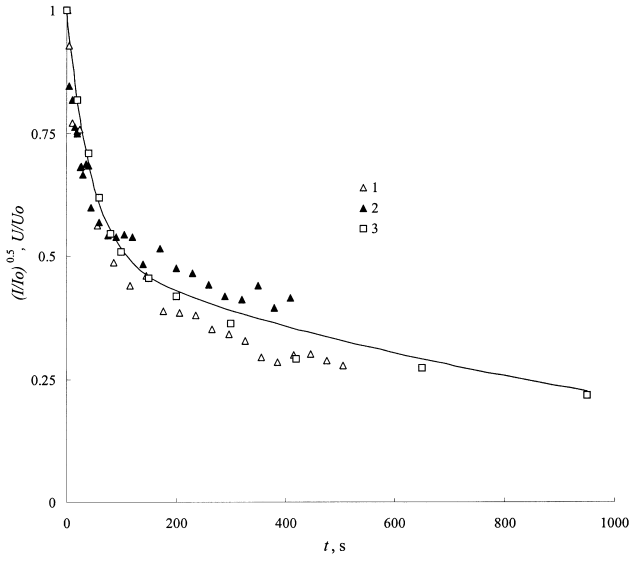

Fig. 5. The $(I/I_0)^{0.5}$ decay measured at room temperature: (1) before heating and (2) after heating (see text). The 16 vol.% PEO/PMMA blend contains 0.4 M of DO-3. (3) The U/U_0 decay in the dopant-free blend. The solid curve follows Eq. (1) and α, τ_{e1} and τ_{e2} are given in Table 2.

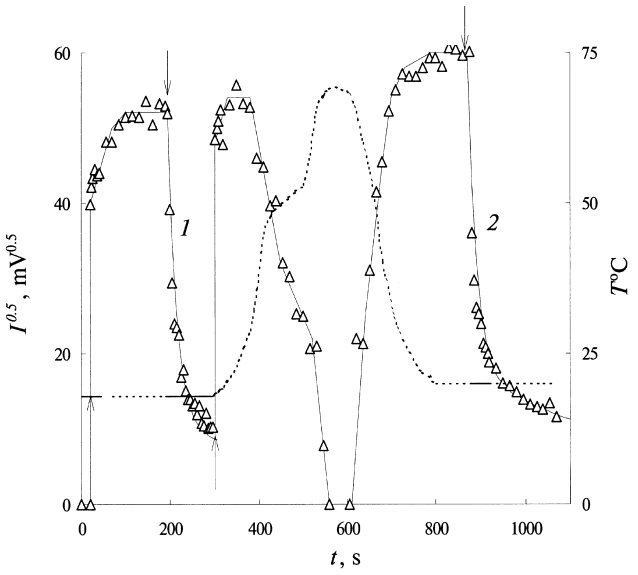

Fig. 6. The temporal dependence of $I^{0.5}$ (solid line) after switching the corona discharge on and off (arrows up and down, respectively) for the 25 vol.% PEO/PMMA blend containing 0.4 M of DO-3. The dotted line shows the specimen temperature.

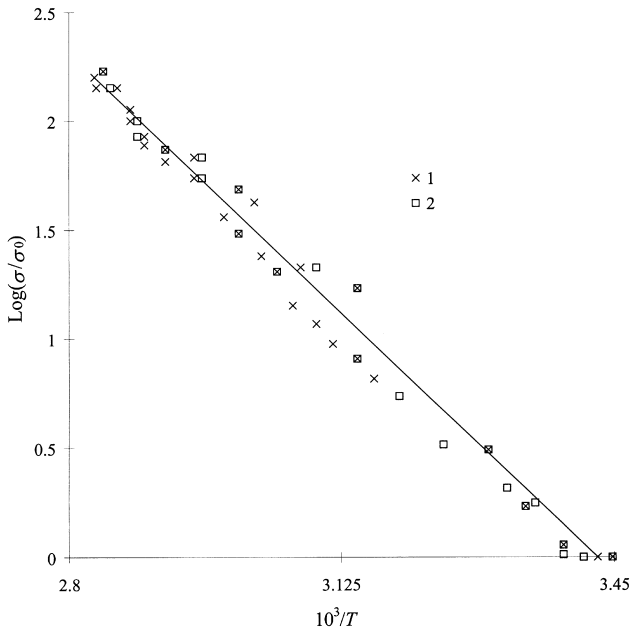

Fig. 7. The temperature dependence of the DC conductivity, σ/σ_0, for 25 vol.% PEO/PMMA blends, both containing: (1) 0.4 M DO-3 and (2) dopant-free. σ_0 is the conductivity at room temperature.

coincide with the U/U_0 decay curve. They also correspond to Eq. (1) with $\alpha = 0.7$, $\tau_{e1} = 20$ s and $\tau_{e2} = 500$ s (see Table 2). A reduction in the SH signal on heating is observed in the blend containing 25% PEO. It is induced by the sharp decay of the surface potential. This conclusion is based on the temperature dependence of conductivity of the 25% PEO/PMMA blends (both undoped and doped with 0.4 M DO-3) as given in Fig. 7. The temperature dependence of σ/σ_0 is reversible (σ_0 is the conductivity at 20°C), that is σ goes back to σ_0 when the temperature decreases to room temperature. The conductivity of the polymer blend increases by two orders of magnitude when the temperature is increased from 20 to 65°C (Fig. 7). According to Eq. (3) this induces a considerable decrease in the surface potential, U_0, and hence in the poling field E_0.

Table 2 shows the increased contribution of the fast term α and shortening relaxation times τ_{e1} and τ_{e2} with increasing the PEO content, trends similar to the behaviour of PMMA containing NDMA.

The bi-exponential decay of the surface potential U/U_0 (and hence $(I/I_0)^{0.5}$) may be explained by a process that is similar to the one for PMMA containing NDMA. The broad distribution of microcavity free volume sizes in the PEO/PMMA blends noted above [15] agrees with the granular texture of the polymer in which the dense grains are interconnected by less-dense interfacial zones [23]. The above mentioned growth of V_{max} with the increasing PEO content [15] confirms the relative increase of the interfacial zone size. Thus the increase in the fast term contribution α and the shortening of τ_{e1} with the increasing PEO content shown in Table 2 may be caused by a corresponding increase in the contribution of the self-trapped charge in the interfacial regions. The τ_{e2} shortening may be explained by the growth in ionic conductivity as the PEO content is increased.

In order to reveal the relaxation due to rotation of DO-3 molecules and to establish the possible dependence of this process on physical ageing it is necessary to decrease τ_e leaving τ_{rot} unchanged. This was achieved by adding molecules promoting hole transport. The 2% PEO/PMMA blend having the lowest free volume fraction and conductivity was additionally doped with centrosymmetrical molecules of 4-diethylamino-benzaldehyde-diphenylhydrazone (DEH) at a concentration of about 0.7 M. Fig. 8 shows the U/U_0 and $(I/I_0)^{0.5}$ decay curves for the blend after switching off the corona discharge. For this composition the U/U_0 decay is distinctly faster than the $(I/I_0)^{0.5}$ decay. The surface potential decay corresponds to Eq. (1) with $\alpha = 0.73$, $\tau_{e1} = 10$ s, $\tau_{e2} = 200$ s and $\alpha = 0.65$, $\tau_{e1} = 10$ s and $\tau_{e2} = 300$ s after storage for 10 days and 5 weeks, respectively. Fig. 8 shows considerable slowing of the $(I/I_0)^{0.5}$ relaxation as compared with the U/U_0 decrease (compare plots 5 and 1). Additionally, the $(I/I_0)^{0.5}$ decay is slowed down as a result of ageing at room temperature after a temperature excursion to 75°C for 5 min followed by rather rapid cooling (compare plot 5 with plots 7 and 8).

A study of physical ageing and glass transition for the present PEO/PMMA blends was reported in a separate paper [27]. From the present study we may assume that T_g (determined enthalpically, mid-point construction) is around 89°C for the 2% blend. Also in the above-mentioned work isothermal volume contraction was carried out at a temperature slightly below T_g. It was noted that significant ageing takes place. In the present case, a rather complex

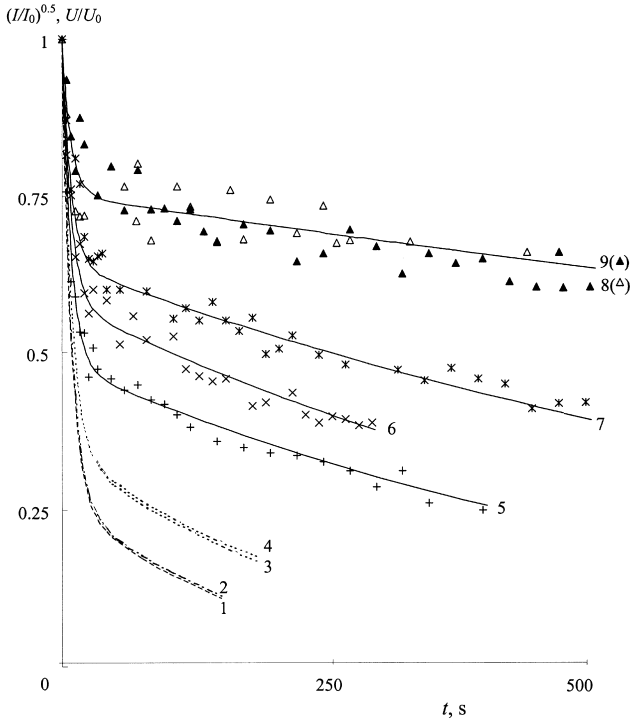

Fig. 8. Effect of ageing time on: (1)–(4) U/U_0 and (5)–(9) $(I/I_0)^{0.5}$ decay curves measured at room temperature for the composition consisting of 2 vol.% PEO/PMMA, 0.7 M DEH and 0.4 M DO-3. Ageing times were: (1) and (5) 38 h, (2) 10 days, (6) and (7) 3 weeks, (3), (4), (8) and (9) 5 weeks; (3), (6), and (8) before heating and (4), (7) and (9) after heating. The heating was carried out at 75°C for 5 min.

temperature history needs to be considered. There is a temperature down-jump to room temperature after poling followed by a temperature up-jump to 75°C. This is followed shortly thereafter by a temperature down-jump to room temperature. It may be assumed that thermodynamic equilibrium was not attained during that time. The blend has a very wide transition region and a broad distribution of relaxation times leading to possible physical ageing effects at temperatures fairly distant from T_g compared to pure polymers. Thus we are dealing with a case where "memory effects" as reported by Kovacs [28] can play a role as a result of a multi-step temperature history. The intention in this work is not to carry out a detailed study of physical ageing but rather to use the SHG technique to analyse the short-term trend when an elevated temperature "impulse" is applied to the optically non-linear system. In addition we present a free volume interpretation possibly explaining the observed time-dependence, keeping in mind that this amorphous system structurally recovers at the temperatures used.

In Fig. 8 the solid lines (5–8) were calculated according to:

$$(I/I_0)^{0.5} = \alpha \exp(-t/10) + (1 - \alpha) \exp(-t/\tau). \quad (6)$$

The fast exponent relaxation time equal to 10 s coincides with τ_{e1} for the U/U_0 decay. EFISH is clearly responsible for the fast component of the $(I/I_0)^{0.5}$ relaxation. In Table 3 the coefficient α and the slow exponent time constant τ in Eq. (6) are given as functions of the ageing time. The relaxation time τ is longer than τ_{e2} and hence should be identified with τ_{rot} in Eq. (4). The relaxation time τ_{rot} increases in the course of the ageing. This effect can be associated with the well-known free volume collapse frequently measured as the external volume contraction on ageing (see for example Vernel et al. [27]). The decrease in the free volume in the interfacial region causes a decrease in the self-trapping charge and hence also a decrease in the coefficient α. As seen in Table 3, α is about 0.25 for the composition after 5 weeks of ageing. It is known that the contribution of the third-order polarisability to the SH signal equals 0.16 for DO-3 molecules [24]. Thus within the experimental error the third-order effect mainly contributes to the fast EFISH component after 5 weeks of ageing.

Table 3
Dependence of α and τ in Eq. (6) on the ageing time. The 2 vol.% PEO/PMMA blend contains 0.4 M DO-3 and about 0.7 M DEH

Ageing time	α	τ (s)
38 h	0.55	800
3 weeks:		
Before heating	0.42	800
After heating at 70°C, 5 min	0.35	1000
5 weeks	0.25	3500

4. Concluding remarks

The well-known optically non-linear PMMA/chromophore system has been extended by blending it with poly(ethylene oxide). Several compositions with 2–25 vol.% PEO in the blend have been studied. The frequently used measurement of the time-dependent SH signal has been carried out in parallel with the surface potential decay measurements in order to better understand the structural mechanisms governing the second harmonic generation. Addition of hole transporting 4-diethylamino-benzaldehyde-diphenyl-hydrazone molecules (DEH) to the optically non-linear composition allowed identification and analysis of the slow mechanism of rotational diffusion.

The dependence of the second harmonic signal strength on the concentration of optically non-linear molecules, the temperature and the blend composition has been investigated. It was found that when the concentration of optically non-linear molecules is high and consequently the mean distance between the molecules is less than 15 Å, these optically non-linear molecules act as hole transport centres and govern the relaxation of both the surface potential and the second harmonic signal. In practical terms the relaxation

time of the second harmonic signal decreases and the decay quickens as the chromophore concentration is increased. When the intermolecular distance is greater than 15 Å (low chromophore concentration) the PEO/PMMA blend has ionic conductivity. The ionic conductivity increases with the increasing PEO content. When the PEO content is increased from 2 to 25% both the second harmonic signal strength and the surface potential relaxation time decrease more than 5×10^4 times. The rotational diffusion relaxation time is always less than τ_e. It has been shown that for a blend with a small (2%) amount of PEO the alignment of the chromophores during the corona discharge is dramatically affected when the temperature is increased to the lower part of the T_g-region, namely to the point where the cubic coefficient of thermal expansion starts to increase. This temperature is much lower than the enthalpic T_g (by mid-point construction).

A multi-step temperature history was carried out for one of the blends (2% PEO). It was found that the rotational diffusion relaxation time increased after 5 weeks of ageing at room temperature. Simultaneously, the fast EFISH component contribution to the second harmonic signal strength decreased almost down to the DC electric-field-induced third-order effect contribution. Based on this work we conclude that the positive information about a mechanism governing the kinetic characteristics of the second harmonic signal decay in the corona discharge poled polymer systems can be obtained only by the simultaneous measurements of both the second harmonic signal and the surface potential.

Acknowledgements

We gratefully acknowledge the grant from the Royal Swedish Academy of Science (project No. 12644), the grant from the International Science and Technology Center (project No. 872-98) and the grant from the Russian Foundation for Basic Research (project No. 99-03-32111).

References

[1] Bauer SJ. Appl Phys 1996;80:5531.
[2] Burland DM, Miller RD, Walsh CA. Chem Rev 1994;94:31.
[3] Hampsch HL, Torkelson JM, Bethke SJ, Grubb SG. J Appl Phys 1990;67:1037.
[4] Guan HW, Pauley MA, Brett T, Wang CH. J Polym Sci, Part B: Polym Phys 1994;32:2615.
[5] Guan HW, Pauley MA, Wang CH. Bull Am Phys Soc 1995;40:158.
[6] Ye C, Minami N, Marks TJ, Yang J, Wong GK. Macromolecules 1988;21:2899.
[7] Wang CH, Guan HW, Gu SH. J Non-Cryst Solids 1993;172:705.
[8] Guan HW, Wang CH, Gu SH. J Chem Phys 1994;100:8454.
[9] Goodson T, Wang CH. J Phys Chem 1996;100:13 920.
[10] Pauley MA, Guan HW, Wang CH. J Chem Phys 1996;104:6834.
[11] Liu L-Y, Ramkrishna D, Lackritz HS. Macromolecules 1994;27:5987.
[12] Vannikov AV, Klason C, Mal'tsev EI, Rychwalski RW, Savel'ev VV. Polym Sci Ser A 1997;39:705.
[13] Vannikov AV, Grishina AD, Rychwalski RW, Ponomarenko AT. Russ Chem Rev 1998;67:451.
[14] Vannikov AV, Vernel J, Mal'tsev EI, Savel'ev VV, Rychwalski RW. Polym Engng Sci 1999;39:261.
[15] Wästlund C, Maurer FHJ. Macromolecules 1997;30:58.
[16] Wästlund C, Schmidt M, Schantz S, Maurer FHJ. Polym Engng Sci 1998;38:1286.
[17] Vernel J. Department of Polymeric Materials, Chalmers University of Technology, SE-421 96 Göteborg, Sweden. Unpublished results.
[18] Oudar JL, Chemla DS. Opt Commun 1975;13:164.
[19] Nicoud JF, Twieg RJ. In: Chemla DS, Zyss J, editors. Nonlinear optical properties of organic molecules and crystals. New York: Academic Press, 1987 (chap. 4).
[20] Blythe AR. Electrical properties of polymers. Cambridge: Cambridge University Press, 1979.
[21] Scharfe M. Electrophotography principles and optimization. Letchworth, England/New York: Research Studies Press/Wiley, 1984 (p. 101).
[22] Das-Gupta DK. IEEE Trans Electr Insulation 1990;25:503.
[23] Lindsay GA, Henry RA, Hoover JM, Knoesen A, Mortazavi MA. Macromolecules 1992;25:4888.
[24] Dhinojwala A, Wong GK, Torkelson JM. J Opt Soc Am B 1994;11:1549.
[25] Brower SC, Hayden LM. J Polym Sci, Part B: Polym Phys 1998;36:1013.
[26] Brower SC, Hayden LM. J Polym Sci, Part B: Polym Phys 1995;33:2391.
[27] Vernel J, Rychwalski RW, Pelisek V, Saha P, Schmidt M, Maurer FHJ. Thermochim Acta 1999;342:115.
[28] Kovacs AJ. Fortsch Hochpolym-Forsch 1955;7:30.